JGR Oceans

RESEARCH ARTICLE
10.1029/2018JC014786

Air-Sea Gas Transfer: Determining Bubble Fluxes With In Situ N_2 Observations

Steven Emerson[1], Bo Yang[1,2], Mariela White[1], and Meghan Cronin[3]

[1]School of Oceanography, University of Washington, Seattle, WA, USA, [2]Now at Department of Environmental Sciences, University of Virginia, Charlottesville, VA, USA, [3]Pacific Marine Environmental Laboratory, Seattle, WA, USA

Key Points:
- Bubble-promoted, air-sea gas transfer is an important part of the annual oxygen flux in regions with high winds
- Ten monthlong periods of in situ N_2 and O_2 gas measurements in the subarctic Pacific are used to verify a recent bubble flux model
- The model overpredicts the bubble flux for N_2 and by inference other insoluble gases; a correction factor of 0.37 ± 0.14 is proposed

Supporting Information:
- Supporting Information S1

Correspondence to:
S. Emerson,
emerson@u.washington.edu

Citation:
Emerson, S., Yang, B., White, M., & Cronin, M. (2019). Air-sea gas transfer: Determining bubble fluxes with in situ N_2 observations. *Journal of Geophysical Research: Oceans*, *124*, 2716–2727. https://doi.org/10.1029/2018JC014786

Received 20 NOV 2018
Accepted 5 MAR 2019
Accepted article online 13 MAR 2019
Published online 21 APR 2019

Abstract Oxygen measurements by in situ sensors on remote platforms are used to determine net biological oxygen fluxes in the surface ocean. On an annual basis these fluxes are stoichiometrically related to the export of organic carbon from the upper ocean (the ocean's biological carbon pump). In situ measurements on remote platforms make it feasible to observe the annual biological oxygen flux globally, but the accuracy of these estimates during periods of high winds depends on model-determined fluxes by bubble processes created by breaking waves. We verify the importance of bubble processes in the gas exchange model of Liang et al. (2013, https://doi.org/10.1002gbc.20080) using surface-ocean N_2 gas measurements determined from observations of dissolved gas pressure and oxygen concentrations every 3 hr on a mooring in the northeast subarctic Pacific at Ocean Station Papa. The changes in N_2 concentration during 10 separate monthlong periods in the winters between 2007 and 2016 indicate that bubble processes in the gas exchange model are over predicted by about a factor of 3 at this location. (The bubble mass transfer coefficients must be multiplied by 0.37 ± 0.14 to match the observations.) These results can be used to adjust model-determined bubble fluxes to yield more accurate measurements of net biological oxygen production until the next generation gas-exchange models are developed.

Plain Language Summary The flux of oxygen from the ocean to the atmosphere is related to the net biological flux of carbon to the ocean's interior. The biological carbon flux is the key process that determines the concentration of CO_2 in the atmosphere and the oxygen concentration of deep ocean water. The net biological oxygen flux at the ocean-atmosphere interface can be determined by measuring the gradient of oxygen across the air-water interface and using this value in models of air-sea gas exchange rates. To determine the biological component of the oxygen flux, the models must be able to evaluate physical fluxes of gas transfer caused by bubbles that result from breaking waves at high wind speeds. Our paper uses measurements of nitrogen gas on a surface mooring in the northeast Pacific Ocean to evaluate the role of bubbles in air-sea gas exchange. With the information provided here oceanographers can use the verified gas exchange models to accurately determine biologically produced air-sea oxygen fluxes. This advance will make it possible to verify biological fluxes that are critical for determining the ocean's role in climate, predicted in global circulation models.

1. Introduction

The mass balance of oxygen in the upper ocean is used to determine local values of annual net community production (ANCP), which is the driving force for the ocean's biological pump. The air-sea exchange rate is the most important physical flux in the upper ocean mass balance, and it is modeled by envisioning two mechanisms: diffusive transport across the air-water interface driven by the difference in partial pressures of the gases in the air and water and a process that enhances the exchange at high winds caused by the creation of bubbles created when waves break. The bubble process is far more important for the insoluble atmospheric gases (N_2, O_2, and Ar) than for CO_2, but it has never been adequately quantified for air-sea carbon exchange.

The utility of upper-ocean oxygen mass balance for determining rates of biological processes (Figure 1) was developed at ocean time series stations and on ships of opportunity where it was possible to determine a seasonal cycle of oxygen along with other inert gases, usually Ar or N_2 (e.g., Cassar et al., 2009; Emerson & Stump, 2010; Hamme & Emerson, 2006; Palevsky & Quay, 2017; Spitzer & Jenkins, 1989; Stanley et al., 2009). If the concentration of an inert gas is determined along with oxygen, it is a tracer for physical

©2019. American Geophysical Union. All Rights Reserved.

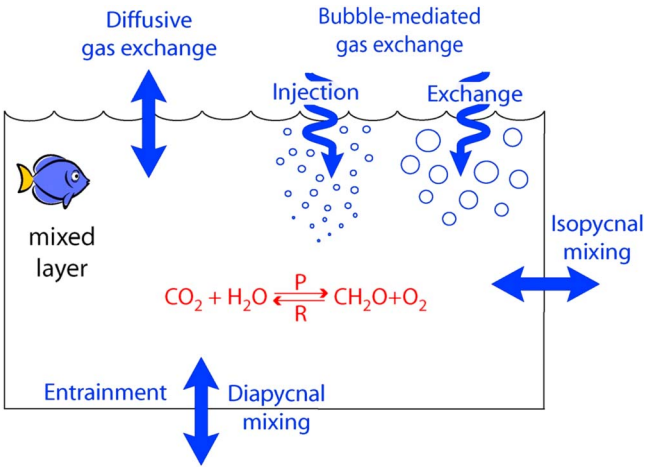

Figure 1. A schematic of the upper ocean indicating mechanisms that affect the oxygen mass balance. Both air-water interface gas exchange (equation (2)) and bubble processes (equations (5) and (6)) are indicated. The equation in the figure is a simple representation of photosynthesis (P) and respiration (R) where CH_2O is a shortened form for organic matter.

processes affecting the saturation state, and it is unnecessary to use a model to determine the role of bubbles. Now that it is possible to determine accurate oxygen concentrations in situ on profiling floats and gliders, the number of annual oxygen time series has expanded dramatically. Interpreting these data in terms of biological fluxes, however, requires an accurate model of the influence of bubble processes at high winds because it is presently not possible to measure inert gases on autonomous platforms. An example of the importance of bubbles in the annual oxygen flux is in the subarctic Pacific where the annual bubble flux to the ocean is about the same as that produced in the mixed layer by biological processes (Bushinsky & Emerson, 2015).

The purpose of this paper is to verify the most current and complete model of the role of bubbles in air-sea gas exchange (that of Liang et al., 2013, hereafter L13) using nitrogen gas concentrations determined on a mooring in the subarctic Pacific at Ocean Station Papa (OSP; 145°W, 50°N). We show that the current model overpredicts the flux of bubbles at high wind speeds and suggest a correction factor to be used until there is further verification and/or refinement of the model

The paper begins with a short background discussion of air-sea gas exchange models and their observational backing. We then describe the time series of N_2 gas observations in the surface ocean at OSP. This is followed with a description of the model used to interpret the results, and what the data reveal about the prediction of bubble fluxes. We end with a discussion of the most important uncertainties in our interpretation of the data.

2. Background

2.1. Gas Exchange Models

Predicting air-sea gas exchange is presently an imperfect combination of empirical measurements of gas tracers in the ocean and simple models of atmosphere-ocean gas transfer. The general formula for air-water gas exchange in nature includes two separate fluxes: one describing exchange at the air-water surface, F_S, and one that predicts the contribution due to bubbles created by breaking waves, F_B:

$$F_{\mathrm{A-W}} = F_{\mathrm{S}} + F_{\mathrm{B}}. \tag{1}$$

The flux at the air-water surface of a gas, G, with concentration $[G]$ (mol/m^3) is modeled by an expression analogous to Fick's second law of diffusion in which the flux is the product of a mass transfer coefficient for gas G, $k_{\mathrm{S,G}}$ (m/day), and the air-sea concentration or partial pressure difference, where $[G^{\mathrm{sat}}]$ is the gas concentration in equilibrium with the atmospheric fugacity, f_G^a and $K_{H,G}$ is the Henry's law constant (mol·m^{-3}·atm^{-1}).

$$F_{\mathrm{S}} = -k_{\mathrm{S,G}}\left\{[G]-\left[G^{\mathrm{sat}}\right]\right\} = -k_{\mathrm{S,G}}K_{\mathrm{H,G}}\left\{f_G^w - f_G^a\right\} \tag{2}$$

The relationship between the atmospheric fugacity, total atmospheric pressure, P^a, and the mole fraction of the gas in the atmosphere, X_G, is

$$f_G^a = P^a\left(1-p_{H_2O}\right)X_G. \tag{3}$$

See Emerson and Hedges (2008, Chapter 10) for details about different models of interface gas exchange.

The flux created by bubbles has been described in many ways (e.g., Fuchs et al., 1987; Keeling, 1993; L13; Merlivat & Memery, 1983; Woolf, 1997; Woolf & Thorpe, 1991). We adopt the model of L13 who used the formulism for gas transfer by bubbles of Fuchs et al. (1987) in a high-resolution three-dimensional model of the upper ocean, which created bubbles by wave processes. Emerson and Bushinsky (2016) showed that the L13 model was consistent with the measured saturation anomalies for noble gases and N_2 in the ocean thermocline and that these data could not be reproduced using models that did not include bubble processes.

The bubble model of Woolf (1997) was also able to account for the noble gas measurements, but it does not distinguish separate mechanisms for different bubble sizes, and Vagle et al. (2010) showed that this model greatly over predicted N_2 saturation at OSP. We adopt the L13 model because it stems from a high-resolution three-dimensional model of air-sea interaction, and it is being continuously upgraded (e.g., Liang et al., 2017).

The bubble models of Fuchs et al. (1987) and L13 assume that the full spectrum of bubbles can be described by a combination of two bubble transfer processes:

$$F_B = F_C + F_P. \tag{4}$$

The first mechanism, F_C, is for small bubbles, <50 μm in diameter, that collapse and inject their contents into the water. (The subscript C here refers to the collapse.) In this case the flux of gas depends only on the total volume of air transferred by these small bubbles, which is described by the product of an empirical transfer velocity, k_C, (mol·m^{-2}·day^{-1}) and the mole fraction of gas G in the atmosphere, X_G:

$$F_C = k_C X_G. \tag{5}$$

This flux is a one-way transfer into the ocean. The behavior of small bubbles in the surface ocean is not well understood because of the difficulty of measuring them, and studies of the volume scattering function indicate that some of bubbles this size may be stabilized by organic coatings (Zhang et al., 2002). Nonetheless, the saturation anomalies of noble gases and N_2 in the ocean require a formulation like that in equation (5) to explain the results (Hamme et al., 2017).

The second bubble mechanism called "exchange" or "partial trapping," F_P, depicts the process of bubble transfer caused by larger bubbles, 50–500 μm in diameter, that do not collapse but instead exchange gases across the bubble-water interface and then rejoin the atmosphere. The model of this process depends on two unknowns: the mass transfer coefficient, k_P (m/day), and the fractional over pressure of the gas in the bubble, ΔP, compared to the atmospheric pressure, P^a, caused by hydrostatic pressure and surface tension.

$$F_P = k_P \left\{(1 + \Delta P)\left[G^{sat}\right] - [G]\right\} \tag{6}$$

The air-sea gas exchange model for gas G can thus be expressed as

$$F_{A-W} = -k_S\left([G] - \left[G^{sat}\right]\right) + k_C X_G + k_P\left\{(1 + \Delta P)\left[G^{sat}\right] - [G]\right\}, \tag{7}$$

where each of the unknowns, k_S, k_C, k_P, and ΔP, has their own individual dependence on wind speed. These dependencies are described in L13 and in the appendix of the paper by Emerson and Bushinsky (2016), where the model predictions are compared to inert gas data in the ocean thermocline.

2.2. The Gas Exchange Mass Transfer Coefficients, k_S

Values for the mass transfer coefficient of the air-water interface exchange, k_S, have been determined repeatedly using ocean tracer data. The most prominent of these is the injection of purposeful tracers into the surface ocean followed by measurements of the concentration of the tracers as a function of time (Watson et al., 1991). Concentration decreases are caused by mixing with tracer-free surrounding waters and by gas flux to the atmosphere. Two tracers are employed so both unknowns can be determined. The gases ^{3}He and sulfur hexafluoride (SF_6) have been used as the tracers most often in these experiments because they meet the criteria of being detectable at very low levels, having virtually no natural background, and being inert in the aquatic environment.

The mass transfer coefficients from all dual tracer experiments to date are plotted versus wind speed in Figure 2. The Y axis value, k_{660}, is the mass transfer coefficient determined from the gases SF_6 and ^{3}He using the model in equation (2). The value of k_S is normalized to the Schmidt number for CO_2 in seawater at 20 °C ($Sc_{,CO2} = 660$, thus k_{660}). The best fit line of Ho et al. (2011) is presented in the figure. (Earlier curves through the tracer-release experiments of Wanninkhof, 1992, and Nightingale et al., 2000, are only slightly different from that of Ho et al., 2011). Three other curves in Figure 2 describe values of k_{660} from experiments in which there is no contribution from bubbles. The line labeled LM86 is the middle leg of the gas exchange

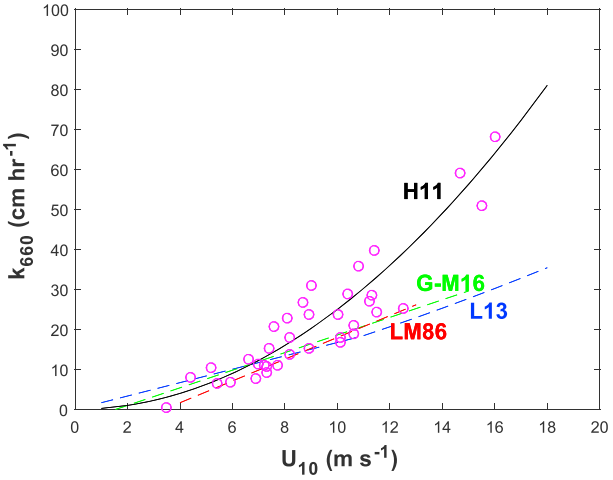

Figure 2. The gas exchange mass transfer coefficient normalized to the Schmidt number for CO_2 at 20 °C and $S = 35$, k_{660}, versus wind speed at 10 m above the sea surface, U_{10}. Symbols represent the results from purposeful tracer release experiments (Ho et al., 2011). Lines are regressions for the mass transfer coefficient as a function of wind speed suggested by Ho et al. (2011; H11) from the purposeful tracer experiments; Goddijn-Murphy et al. (2016; G-M16) based on atmosphere eddy correlation measurements of dimethyl sulfide over the ocean; the second limb of the linear correlations of Liss and Merlivat (1986; LM86), which derive from the purposeful tracer release in a lake (Wanninkhof, 1985); and the formula presented for the COAREG model (Fairall et al., 2008), which was used in the air-sea exchange model of Liang et al. (2013, L13).

relationship from Liss and Merlivat (1986) that originated from a tracer release experiment in a small sheltered lake by Wanninkhof et al. (1985). The line labeled G-M16 (Goddijn-Murphy et al., 2016) is from eddy covariance measurements of dimethyl sulfide (DMS) over the ocean. Bubble processes have diminishing importance for highly soluble gases because most of the gas is in solution already and DMS is so soluble in water that the contribution to gas exchange from bubbles, even at high winds, is very small. The third line labeled L13 is from the formula suggested in the NOAA COAREG air-sea exchange model (Fairall et al., 2008). This is the wind speed relationship used by L13 for k_s in their model, and the one we use here to be consistent. Clearly, all three of these "no bubble gas exchange" mass transfer formulations are very similar and the same, within the scatter of the data, to the results of the tracer release experiments until wind speeds exceed of 8–10 m/s when the tracer release results become greater as the U_{10} increases.

The difference between the tracer-release experiments and the linear relationships determined in the absence of bubbles is caused by the conditions at high winds. A caveat here is that only the DMS trend is based on data where wind speeds were greater than 8–10 m/s and then only to U_{10} ~ 15 m/s. In the models presently used in oceanography, the differences in the mass transfer coefficient trends at wind speeds above 8–10 m/s is the result of bubbles, but we should keep in mind that this is just a model and the actual mechanisms could involve more processes.

In the case of the tracer release experiments concentrations of SF_6 and ^3He in the ocean are far greater than natural values in the atmosphere, so the flux described in equation (7) can be greatly simplified. There is no contribution from small bubbles because there is no tracer in the atmosphere, so F_C ~ 0, and $[C] >> [C^{sat}]$ because of the artificial tracer addition. This leaves the tracer-release air-sea flux to be

$$F_{A-W} = -k_{S,G}\,[G] - k_P\,[G] = -\left(k_{S,G} + k_P\right)\,[G]. \quad (8)$$

The value of k_{660} from the tracer-release experiments in Figure 2 is a combination of values determined by the air-sea flux and large bubbles that incorporate gas tracer from the water while in the ocean and ferry it to the atmosphere when they ascend to the surface. The departure of the two lines above $U_{10} = 8$–10 m/s is due to the gas exchange process in large bubbles. This process is difficult to separate from that at the air-sea surface, since they both depend on molecular diffusion across an interface (i.e., Hamme et al., 2017). One cannot determine the entire mechanism for large bubble exchange from the data in the figure because the purposeful tracer releases give no information about the value of the pressure inside large bubbles, ΔP, which is very important for transfer of insoluble atmospheric gases (N_2, O_2, Ar, and noble gases) to the ocean by large bubbles.

The data in Figure 2 suggest that the effect of bubbles in air-sea gas transfer becomes important in regions of the ocean where wind speeds are greater than 8–10 m/s. A map of the percent of time during a year in which wind speeds over the ocean are greater than 10 m/s (Figure 3) indicates that bubble processes are most important at latitudes greater than about 40°. In the subtropics bubble processes are not likely to have much effect, but in the subarctic regions they play an extremely important role.

In situ measurements of N_2 have been used previously to determine the role of bubbles in air-sea gas exchange (e.g., Emerson et al., 2002; McNeil et al., 1995; Vagle et al., 2010). Vagle et al., 2010 used measurements of O_2 and N_2 over three several-day periods at OSP to determine the gas exchange mass transfer coefficients for interface gas exchange (k_S, equation (1)) and a single bubble mass transfer coefficient. They found that bubble processes using the model of Woolf (1997) over predicted the observed N_2 concentration increases. Our approach is different from that of Vagle et al. (2010) in more ways than the bubble model we use. We interpret only the N_2 data (because biological processes can affect the change in concentration

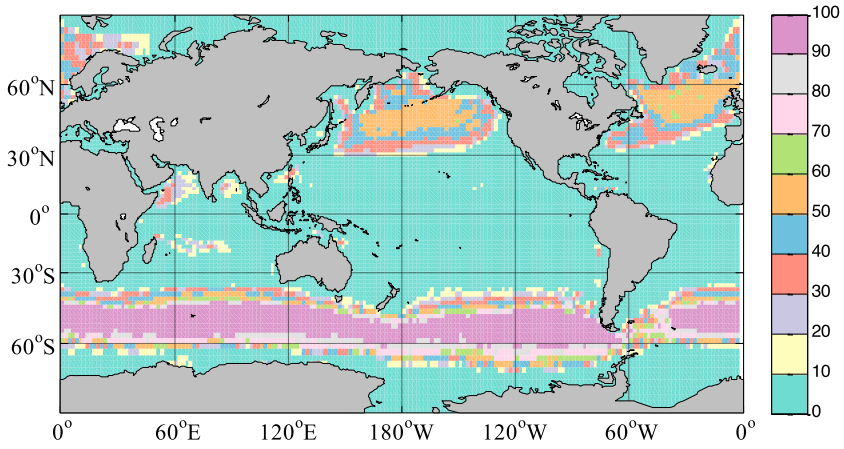

Figure 3. Fraction of the year when weekly mean wind speed at 10-m height, U_{10}, exceeds 10 m/s. The data are compiled from NOAA-CIRES 20th Century Reanalysis version 2c.

of O_2), we adopt k_s from previous tracer-release and eddy correlation studies, and we interpret data from 10 monthlong wintertime periods over a period of 10 years. Other improvements of our experimental approach are simultaneous measurement of the pressures of both the atmospheric and dissolved gases—the first on the tower of the mooring and the second in the gas tension device (GTD), and careful calibration of the in situ oxygen sensor so that the total gas pressures can be used to yield accurate nitrogen gas measurements.

3. Observation Methods

The data of surface ocean N_2 concentration that we use to calibrate the L13 bubble model were derived from a CTD-GTD-O_2 instrument attached to the bridle of a surface mooring at the Canadian time series station at OSP (145°W, 50°N). The CTD part of the instrument is a Seabird 19+ CTD (temperature, salinity, and hydrostatic pressure sensor). The GTD is a Paroscientific pressure sensor housed in a chamber behind a ridged template with a small hole covered by a silicon membrane and is used to measure the total gas pressure dissolved in the water (McNeil et al., 1995). The O_2 sensors used are an Aanderaa optode with a SBE-43 Clark electrode as a backup. The mooring at OSP is part of the NOAA Ocean Climate Stations project and is described in Cronin et al. (2015). A photograph of the instrument attached to the bridle of the surface mooring is presented in Figure 4. The mooring is renewed annually in June, and the data we describe span a 10-year period from 2007 to 2016.

The suite of in situ measurements determined on the mooring are T, S, O_2 concentration, and total gas pressure in the surface water with accompanying atmospheric pressure and wind speed measurements on the buoy tower every 3 hr. Methods used to determine [N_2] concentration from measurements of gas tension and oxygen are described by Emerson et al. (2002). Briefly, highly accurate measurements of atmospheric pressure, along with total gas pressure and pO_2 in surface waters, make it possible to determine accurate concentrations of nitrogen gas in the water because N_2 and O_2 make up about 95% of the total gas pressure in a wet atmosphere. It is assumed that the gas pressures of both argon and H_2O gas, constituents that make up most of the remaining gas pressure, are at saturation equilibrium in surface ocean waters. Atmosphere and GTD pressures are measured with Paroscientific Sensors that have accuracies quoted by the manufacturer of ±0.01%. Assuming these accuracies are correct and that the pO_2, pAr, and pH_2O are known with an accuracy of ±1.0%, the nitrogen gas pressure can be determined to an accuracy of ±0.2%. By far the largest error in the [N_2] measurement by this method is the accuracy of the concentration or partial pressure of oxygen in the surface waters (see Emerson et al., 2002).

Oxygen sensors are known to have inaccurate factory calibrations and to drift in the upper ocean (see Bushinsky et al., 2016; Emerson et al., 2002). The optodes we deployed were calibrated in our laboratory periodically during the 10-year period of measurements using the methods described in Bushinsky et al. (2016) and in the field by comparison to oxygen concentrations measured using Winkler titrations. Precautions

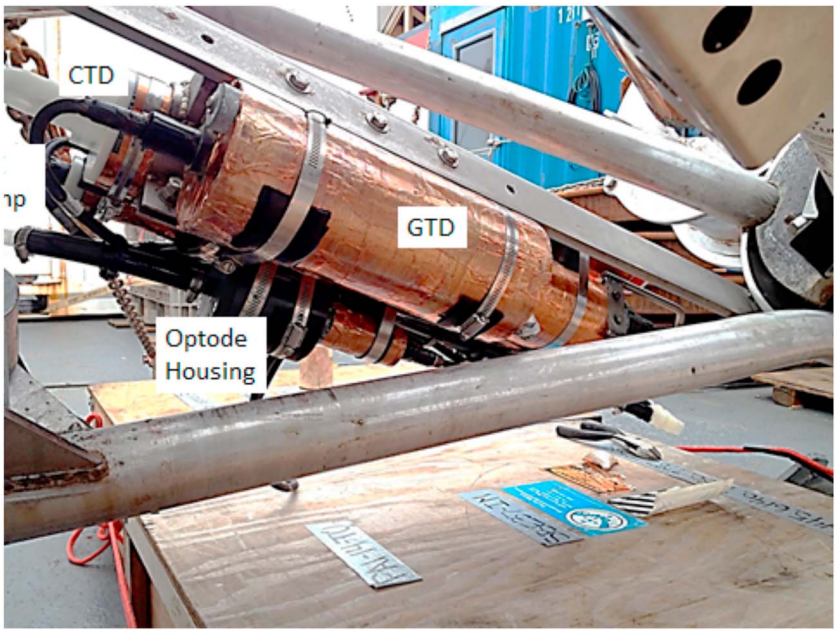

Figure 4. CTD-GTD-O_2 instrument mounted on the bridle of the surface mooring destined for deployment at Ocean Station Papa. The instruments are covered with copper tape to discourage biological fouling, and the Aanderaa oxygen sensor is mounted inside a copper-lined housing, which is flushed with ambient water prior to making the measurement. GTD = gas tension device.

about the accuracy of the Winkler titrations described in Emerson et al. (1999) were followed. The ocean calibrations were done on deployment and retrieval of the moorings (June) and at two intermediate occupations (August and February) by the Canadian Institute of Ocean Sciences time series program. The oxygen data and the calibrations are presented in Table S1 in the supporting information. We believe that with the Winkler calibrations, we achieve accuracy of the oxygen sensor of better than ±1%. All data used in this paper are logged at the online data facilities presented in the "Acknowledgements" section at the end of the paper.

4. Results

The surface ocean nitrogen saturation anomaly is defined as $\Delta N_2(\%) = (\{[N_2]-[N_2^{sat}])/[N_2^{sat}]\} \times 100)$, where the nitrogen saturation values are those determined by Hamme and Emerson (2004) at one atmosphere and are corrected for atmospheric pressure using data from the mooring pressure sensor. Surface water $\Delta N_2(\%)$ between 2007 and 2016 are presented in Figure 5. The tick marks on the *x* axis are placed at 1 January of each year. Many of the deployments begin after a gap in the data because the CTD-GTD-O_2 instrument sometimes did not continue to record for a full year because of battery failure or fouling. The kinds of problems we

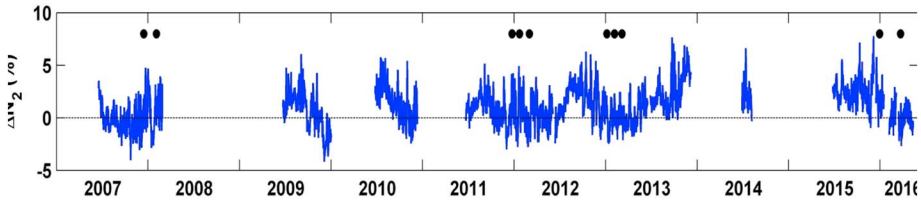

Figure 5. The nitrogen saturation anomaly, ΔN_2 (%) = (([N_2]-[N_2^{sat}])/[N_2^{sat}]) × 100 in the surface ocean (~2 m) of the subarctic Pacific (Ocean Station Papa) for a period of 10 years. Tick marks are 1 January of each year. The mooring was deployed and recovered in June. Gaps in the data are times when the CTD-GTD-O_2 instrument stopped recording. Dots indicate the monthlong wintertime periods used to calibrate the bubble model. GTD = gas tension device.

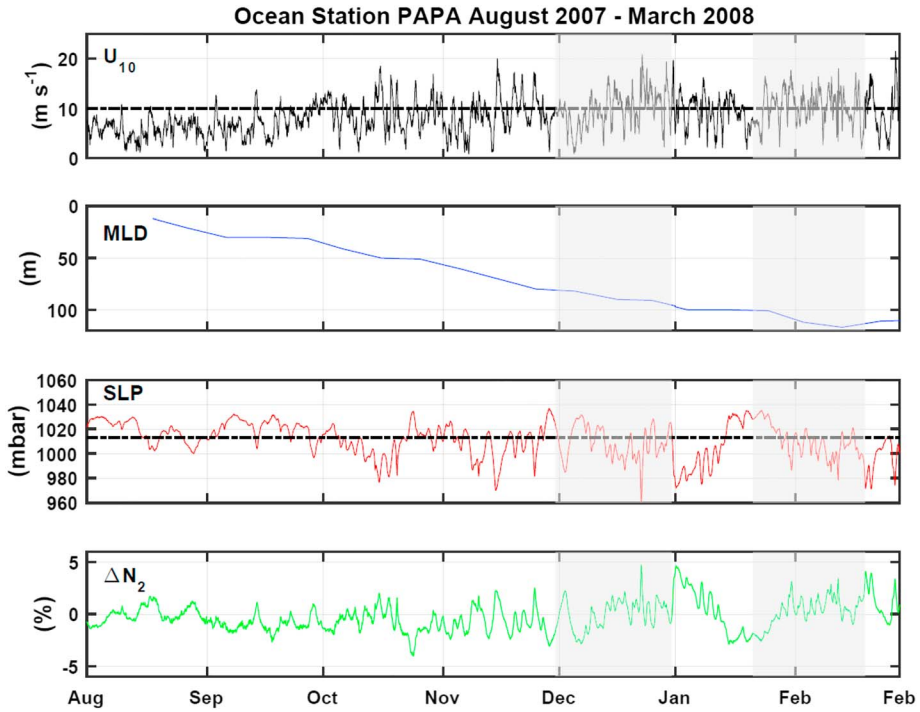

Figure 6. An example of mooring measurements during the 2007/2008 period. U_{10} is the wind speed at 10-m height measured on the mooring tower. MLD is the mixed layer depth determined from Argo floats in the area (see text). SLP is the sea level pressure in millibars (1 atm. = 1,013 mbar) determined on the tower of the mooring. ΔN_2 is the nitrogen saturation anomaly in percent determined with the CTD-GTD-O_2 instrument in the mooring bridle. ΔN_2 equal zero is equilibrium with the atmosphere, positive is supersaturation, and negative is undersaturation. Periods used to calibrate the bubble model are indicated by gray shading.

encountered are exemplified by an instance (in 2013) in which barnacles seeded under a plastic tie-wrap holding deep-sea electrical cables together, and as they grew, they cut their way into the cable until the system shorted. Because redeployments took place in June and the instrument invariably lasted at least 6–8 months, there are data during most winter periods when the high winds occur. The general trend in the data (Figure 5) is for N_2 supersaturation in the summer because of warming of the surface ocean, which gives way to large fluctuations around zero in the winter. Much of the very rapid change in ΔN_2 in wintertime is due to the great variability in atmospheric pressure accompanying winter storms. A low-pressure system occurs rapidly in hours or days, and it requires several weeks for gases in a 100-m mixed layer to re-equilibrate with the atmosphere. The 10 dots in Figure 5 show the time of the monthlong winter periods used to calibrate the bubble model.

An example of data in 2007–2008 from August to February (Figure 6) indicates typical annual variability. Wind speeds are mostly under 10 m/s in summer, but in winter they frequently reach highs of 15–20 m/s. The mixed layer depth deepens from a few tens of meters in summer to 100–110 m in winter. There is a permanent halocline at 110 m in the eastern subarctic Pacific that limits the depth of winter mixed layers. Sea level pressure fluctuates between about ±10 mbar of one atmosphere (1,013 mbar) in summer, but in winter values plunge to 980 during storms. Notice the general inverse relationship between ΔN_2 and sea level pressure.

The periods chosen to test the bubble model in 2007–2008 are indicated by shading in Figure 6. The 10 periods we interpret in this paper meet the following criteria: (1) They are in wintertime when winds are strong, and mixed-layer depths are changing very slowly, so that entrainment is of minor importance, and (2) we chose periods of time that are equal to or longer than one N_2 gas exchange residence time but short enough to maximize the importance of local air-sea interaction as opposed to the results from remote storms that are advected into the mooring area. The data will be interpreted using a time-dependent one-dimensional model, so we want to avoid horizontal fluxes as much as possible.

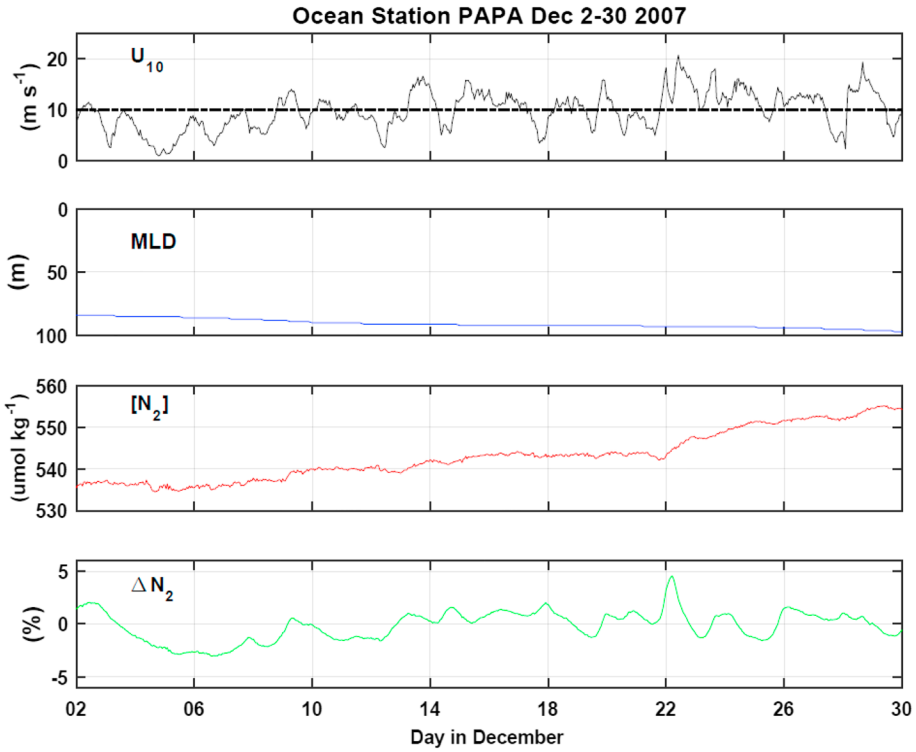

Figure 7. Data used to determine the role of bubbles in winter-time mixed layer over a period of ~30 days in December 2008. The *Y* axes are the same as in Figure 7 except that the N_2 concentration change with time, [N_2], replaces sea level pressure. MLD = mixed layer depth.

A close-up of one of the monthlong periods is presented in Figure 7. Note that the N_2 saturation anomaly is not uniformly undersaturated even though surface waters have been cooling. The saturation anomaly, which is the driving force for air-sea exchange, is dominated by atmospheric pressure changes. The key feature in this figure is the change in nitrogen concentration with time. From the first day in December 2007 to the last day of the month the N_2 concentration increases from 537 to 555 μmol/kg—a change of about 4%. This change is typical of those during each of the ten 1-month periods as illustrated by the figures of N_2 versus time presented in the supporting information.

5. Discussion

5.1. Calibrating Model-Determined Bubble Mass Transfer Coefficients

Model-calculated changes in N_2 are compared with observed trends as a means of determining the strength of bubble-induced increase in nitrogen concentration. We used a one-dimensional model with a mixed layer and 3-m-thick layers below this to 150 m (see Bushinsky & Emerson, 2015; Yang et al., 2018). The model includes processes of air-sea exchange, entrainment, vertical mixing, and vertical advection. For the period of time that we interpret here the only significant fluxes are at the air-sea interface and the vertical flux at the pycnocline (~110 m). The latter value is less than 1.0% of that flux across the air-sea interface, because vertical N_2 gradients at the base of the winter mixed layer are not very great. The concentration-depth profiles are controlled by solubility (see Emerson et al., 2008) and were evaluated for the model based on the temperature and salinity gradients determined from profiling floats. Effectively, the model mass balance is

$$d[\mathrm{N_2}]/\mathrm{d}t \sim F_{\mathrm{A-W}}. \tag{9}$$

From equations (1)–(3)

$$\mathrm{d}[\mathrm{N_2}]/\mathrm{d}t - k_{\mathrm{S,N2}} K_{\mathrm{H,N2}} \left\{ f^{w}_{\mathrm{N2}} - f^{a}_{\mathrm{N2}} \right\} = \beta F_{\mathrm{B}}, \tag{10}$$

$$f^{a}_{\mathrm{N2}} = P^{a} \left(1 - p^{a}_{\mathrm{H_2O}} \right) X_{\mathrm{N2}}. \tag{11}$$

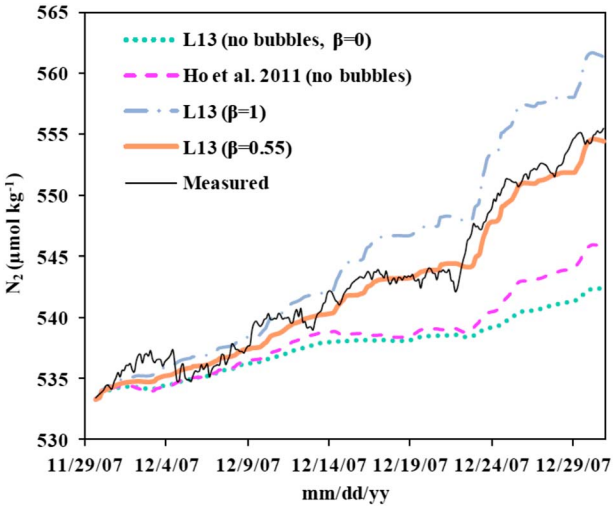

Figure 8. Comparison of model results and observations of the change of $[N_2]$ with time in the surface ocean (0–100 m) at Ocean Station Papa during the month of December 2007. The black solid line is data. Model results without bubbles are the lower green dots and magenta dashed lines. The top blue-dashed-dotted line is the L13 model with no change in the strength of the bubble flux ($ß = 1.0$). The orange solid line is the best fit (for this case $ß = 0.55$). Similar results for the other nine monthlong periods modeled are presented in the supporting information.

The second term on the left side of equation (10) is the air-sea interface flux calculated from the k_{660} values determine from wind speed (Figure 2) and the nitrogen saturation anomaly (Figures 5–7). The partial pressure of water, $p^a_{H_2O}$, in the atmosphere (equation (11)) is determined from National Centers for Environmental Prediction reanalysis and was usually between 80% and 100% saturation near the ocean surface. The value, $ß$, in equation (10) is the tuning parameter used to fit our observations of $[N_2]$ change with time and the bubble flux, F_B, defined in the L13 model. From equation (7),

$$F_B = k_{C,N2}X^{N2} + k_{P,N2}K_{H,N2}\{(1+\Delta P)f^a_{N2} - f^w_{N2}\}. \quad (12)$$

If there were two inert tracers with different solubilities, we could determine a value of $ß$ for each of the bubble mechanism (k_C and k_P), but since there is only one, we assume that the tuning parameters for each of the two mechanisms are equal ($ß_C = ß_P$). Later, we evaluate the potential error associated with this assumption.

An example of the comparison of model results with data from December 2007 is presented in Figure 8. Data are the black lines, and there are four model runs. Green (dotted) and magenta (dashed) lines are model runs without bubble processes ($ß = 0$ in equation (10)). Green is the nitrogen change with time assuming air-sea interface gas exchange characterized by k_s values only (L13 in Figure 2). The magenta line is the same only using the wind speed dependence of k_s from the purposeful tracer experiments (H11 in Figure 2). Clearly, it is not possible to reproduce the data using either of these models without bubble processes. The blue, dash-dotted line is the model result with bubble processes of L13; this is the change expected if $ß = 1.0$. The L13 model overpredicts the effect of bubbles during December 2007 at OSP. The best fit value (the thick orange line) is determined by summing the absolute values of difference between the model and observed nitrogen concentration determined at each time step for runs with $ß$ values between 0 and 1.0. The smallest difference between the model and observations is the best choice of $ß$. The best fit values for each of the 10 wintertime periods are presented in Table 1. Figures analogous to the one for December 2007 (Figure 8) are presented in the supporting information. The last column in Table 1 lists the $ß$ values for each monthlong period of measurements using the assumption that the correction factor is equal for the two mechanisms of the bubble process. The mean and standard deviation of the 10 $ß$ values is 0.37 ± 0.14.

Table 1
Best Fit Values for the Bubble Process Correction Factor, ß, for 10 Different Wintertime Periods at OSP

	$(\beta_c = 2\beta_p)$		$(\beta_p = 2\beta_c)$		$(\beta_c = \beta_p)$
Period	β_p	β_c	β_p	β_c	
07/08-1	0.35	0.69	0.79	0.40	0.55
07/08-2	0.20	0.39	0.45	0.23	0.32
11/12-1	0.30	0.59	0.83	0.42	0.52
11/12-2	0.28	0.55	0.73	0.37	0.47
11/12-3	0.14	0.27	0.28	0.14	0.21
12/13-1	0.22	0.43	0.52	0.26	0.35
12/13-2	0.07	0.13	0.15	0.07	0.11
12/13-3	0.17	0.34	0.47	0.24	0.31
15/16-1	0.16	0.31	0.30	0.15	0.49
15/16-2	0.15	0.30	0.29	0.15	0.33
Mean (std)	0.20 ± 0.08	0.40 ± 0.17	0.48 ± 0.23	0.24 ± 0.12	0.37 ± 0.14

Note. Columns 2 and 3, 4 and 5, and 6 are model results for different assumptions about the relative importance of the correction factor for the two different model bubble processes—small and larger bubbles, β_c and β_p, respectively. OSP = Ocean Station Papa.

Table 2
The ANCP Error Caused by Different Assumptions About the Relative Importance of Model Correction Factors for Small and Large Bubbles: $ß_c$ and $ß_p$, Respectively

			ANCP (OSP; mol C·m^{-2}·year^{-1})			
$ß_c$, $ß_p$ relationship	$ß_c$	$ß_p$	2012–2013	2013–2014	2014–2015	2015–2016
$ß_c = ß_p$	0.37	0.37	2.3 ± 0.6	0.7 ± 0.4	1.9 ± 0.4	1.3 ± 0.4
$ß_p = 2ß_c$	0.24	0.48	2.4	0.7	1.9	1.2
$ß_c = 2ß_p$	0.20	0.40	2.4	0.8	2.0	1.6
$ß_p = 0$	0.52	0.0	2.4	0.9	2.1	1.9
$ß_c = 0$	0.0	0.74	2.4	0.7	1.8	1.0

Note. The range of assumptions are in column 1. $ß$ values are determined from N_2 data at OSP presented in this paper (Table 1). ANCP values in columns 4–7 were calculated from profiling float oxygen data and one-dimensional model presented in Yang et al. (2018). Mean annual wind speeds for the 4 years in columns 4–7 were 8.7, 8.6, 8.7, and 9.6 m/s, respectively. ANCP = Annual Net Community Production; OSP = Ocean Station Papa.

5.2. Error Assessment of the Correction Factor

The roughly ±40% error in the bubble model correction factor, $ß$, probably stems from the simplicity of the assumptions that air-sea gas exchange is a function of wind speed only (e.g., Liang et al., 2017), and our one-dimensional interpretation of upper ocean properties in a swirling, turbulent ocean where storms pass through on a weekly basis. We do not have much choice in adopting these simplistic assumptions because this is the present state of air-sea gas transfer models, and we cannot resolve horizontal gradients with a data set from a single location. Our solution to this problem is to determine the average of an unprecedented number of monthlong winter periods so that we have some measure of variability. We offer three arguments about possible sources of error in the calculation presented here.

A Monte Carlo error analysis of the effect of quantifiable uncertainties of key model variables was performed. We assign the following errors in parameters that determine the air-sea flux (equations (9) and (10)): ±15% in the estimate of k_s, ±0.2% uncertainty in the N_2 concentration, and a ±0.1% error in the atmospheric pressure. The uncertainty estimate for the diffusive gas transfer coefficient stems from the variability in k_s of the three wind speed correlations presented in Figure 2 for U_{10} values of 6–8 m/s. The $[N_2]$ error is based on the accuracy of the N_2 gas measurement described in section 3, and the atmospheric pressure error is 10 times the quoted accuracy of the Paroscientific pressure sensors on the mooring tower. One thousand model runs of randomly varying $[N_2]$ about the measured mean caused a standard deviation around the mean for $ß$ of ±0.01–0.04. Variation of the other parameters by the ranges described resulted in errors for $ß$ in the thousands place and is therefore insignificant. Thus, the maxim error caused by these three uncertainties is in the N_2 gas concentration, and it is at most 10% of the calculated $ß$ values.

It is difficult to quantitatively assess the effects of horizontal advection, but we note that it is the gradient in the saturation anomaly, ΔN_2, not N_2 concentration that is important. Since temperature and N_2 are both advected, it is possible for N_2 and T to have a strong horizontal transport term without affecting the saturation anomaly. Strong gradients in ΔN_2 gas saturation in the surface ocean have not been observed, but they probably exist in ocean frontal regions associated with deep mixed layers. Since the gas exchange residence time in the ocean mixed layer is on the order of weeks to a month, the horizontal footprint of ΔN_2 in a region with mean currents of several tenths of 1 m/s is only a few degrees of latitude or longitude. Since OSP is in the subarctic gyre, it is probably as horizontally homogeneous as any location in the ocean.

The final potential uncertainty we tested is the assumption that the fitting parameter for both bubble mechanisms are equal. There is no reason to expect that this is true; however, with only one tracer we are left with no choice. We evaluated the potential error caused by this assumption by determining β using different assumptions about the relative values of β_c and β_p (columns 2–5 of Table 1). We use these values to determine the effect of the $\beta_c = \beta_p$ assumption on calculating net biological oxygen production from O_2 data at OSP. Oxygen data from Argo floats during the period 2013–2016 are used along with the one-dimensional model described here to determine the net biological oxygen production (see Yang et al., 2018). The results (Table 2) indicate that the value of ANCP determined from the oxygen mass balance at OSP is insensitive to different assumptions about the relative importance of the two bubble mechanisms. The exception is when

$\beta_p = 0$ is assumed a 50% difference is observed for the year with the highest average wind speed, 2015–2016, Not knowing the relative importance of the different mechanisms does not create a large error in the calculation of ANCP by the oxygen mass balance method unless one makes the unrealistic assumption that only one of the bubble mechanisms is operative.

6. Conclusions

Upper-ocean oxygen measurements can be utilized to determine net biological oxygen production if one can quantify the role of physical processes in altering the surface ocean oxygen saturation anomaly. Previous studies of the saturation anomaly of insoluble, inert gases in the ocean indicate that bubble processes are necessary to interpret observations in locations of high winds (e.g., Emerson & Bushinsky, 2016). The difference in wind speed dependence of air-sea gas exchange of highly soluble and insoluble gases (Figure 2) indicates that bubble processes play an important role in surface waters of ocean regions where the wind speeds exceed 8–10 m/s for a significant fraction of the year (Figure 3).

We verify the most recent model of the wind speed dependence of bubble fluxes (L13) using 10 one-month periods of N_2 measurements over a period of 10 years in the subarctic Pacific Ocean, where wind speeds in winter are high enough that bubble processes dramatically affect the air-sea gas exchange mechanisms. A correction factor of 0.37 ± 0.14 is proposed for the mass transfer coefficients of the two bubble mechanisms in the L13 model (Table 1).

It is now possible to confidently determine the biological component of air-sea oxygen fluxes from O_2 data measured on in situ platforms like moorings, profiling floats, and gliders in regions where there are high winds for a significant part of the year. This paper is not the last word on model calculation of bubble processes at the air-sea interface but rather an assessment of our understanding of the process so that O_2 data can be interpreted as accurately as possible while models evolve.

Acknowledgments
We would like to thank scientists at the Institute of Ocean Sciences (IOS) in Sidney, B. C., the Master and crew of the R. V. Tully, and especially Chief Scientist Marie Robert for providing ship space and helping with all aspects of the mooring operation during their regular cruises to OSP. We are grateful to NOAA-PMEL mooring technicians for help in deploying our CTD-GTD-O_2 instrument on the bridle of the surface mooring at OSP. The mooring was funded through NSF grant OCE-0628663 for its first two deployments and thereafter by NOAA's Global Ocean Monitoring and Observing Program. Collaboration with Professor Jun-Hong Liang greatly aided our understanding of his air-sea exchange model. Recent University of Washington research was funded by NSF Grant OCE-1558476. This is PMEL publication number 4841. Data generated and used in this paper are available online. Calibrated N_2 and O_2 data appear along with other results (specifically atmospheric pressure and wind speed) from the NOAA mooring at OSP (https://www.pmel.noaa.gov/ocs/data/disdel/ and https//www.pmel.noaa.gov/ocs/partners-data). Argo data used to determine the surface mixed layer depth in the vicinity of OSP are presented at different websites depending on the year: For 2007–2008 the data are from a float with the WMO ID 4900736 deployed by the department of Fisheries and Oceans, Canada, and logged at http://www.meds-sdmm.dfo.gc.ca/isdm-gdsi/argo/canada/repore-rapport-eng.asp?id=4900726; for the years 2010–2012 data are from a float with the WMO ID: 5903274 deployed by the Monterey Bay Aquarium Research Institute (MBARI) and logged at https://www3.mbari.org/chemsensor/FloatList.html; and finally for the period 2012–2016, data are from a float with the WMO ID 5903743 deployed by the University of Washington and logged at the SOSARGO website (https://sites.google.com/a/uw.edu/sosargo/).

References

Bushinsky, S., & Emerson, S. (2015). Marine biological production from remote in situ oxygen measurements on a profiling float in the subarctic Pacific Ocean. *Global Biogoechemical Cycles*, *29*, 2050–2060. https://doi.org/10.1002/2015GB005251

Bushinsky, S. M., Emerson, S., Riser, S., & Swift, D. D. (2016). Accurate oxygen measurement on modified Argo floats using in situ air calibrations. *Limnology and Oceanography: Methods*, *14*(8), 491–505. https://doi.org/10.1002/lom3.10107

Cassar, N., Barnett, B., Bender, M. L., Kaiser, J., Hamme, R. C., & Tilbrook, B. (2009). Continuous high-frequency dissolved O_2/Ar measurements by equilibrator inlet mass spectrometry (EIMS). *Analytical Chemistry*, *81*(5), 1855–1864. https://doi.org/10.1021/ac802300u

Cronin, M. F., Pelland, N., Emerson, S., & Crawford, W. R. (2015). Estimating diffusivity from the mixed layer heat and salt balances in the North Pacific. *Journal of Geophysical Research: Oceans*, *120*, 7346–7362. https://doi.org/10.1002/2015JC011010

Emerson, S., & Bushinsky, S. M. (2016). The role of bubbles during air-sea gas exchange. *Journal of Geophysical Research: Oceans*, *121*, 4360–4376. https://doi.org/10.1002/2016JC011744

Emerson, S., & Hedges, J. I. (2008). *Chemical Oceanography and the Carbon Cycle*. Cambridge, U.K., New York: Cambridge University Press.

Emerson, S., & Stump, C. (2010). Net biological oxygen production in the ocean II: Remote in situ measurements of O_2 and N_2 in the subarctic Pacific surface waters. *Deep-Sea Research Part I*, *57*(10), 1255–1265. https://doi.org/10.1016/j.dsr.2010.06.001

Emerson, S., Stump, C., Johnson, B., & Karl, D. (2002). Autonomous determination of oxygen and nitrogen concentrations in the ocean. *Deep-Sea Research*, *49*(5), 941–952. https://doi.org/10.1016/S0967-0637(02)00004-3

Emerson, S., Stump, C., & Nicholson, D. (2008). Net biological oxygen production in the ocean: Remote in situ measurements of O_2 and N_2 in surface waters. *Global Biogeochemical Cycles*, *22*, GB3023. https://doi.org/10.1029/2007GB003095

Emerson, S., Stump, C., Wilber, D., & Quay, P. (1999). Accurate measurements of O_2, N_2, and Ar gases in water and the solubility of N_2. *Marine Chemistry*, *64*(4), 337–347. https://doi.org/10.1016/S0304-4203(98)00090-5

Fairall, C. W., Bradley, E. F., Hare, J. E., Grachev, A. A., & Edison, J. B. (2008). Bulk parameterization of air-sea fluxes: Updates and verification for the COARE algorithm. *Journal of Climate*, *16*, 571–591.

Fuchs, G., Roether, W., & Schlosser, P. (1987). Excess ^{3}He in the ocean surface layer. *Journal of Geophysical Research*, *92*(C6), 6559–6568. https://doi.org/10.1029/JC092iC06p06559

Goddijn-Murphy, L., Woolf, D. L., Callaghan, A. H., Nightingale, P. D., & Shulter, J. D. (2016). A reconciliation of empirical and mechanistic models of the air-sea transfer velocity. *Journal of Geophysical Research: Oceans*, *121*, 818–835. https://doi.org/10.1002/2015JD011096

Hamme, H. C., Emerson, S. R., Severinghaus, J. P., Long, M. C., & Yeshayaev, I. (2017). Using noble gas measurements to derive air-sea process information and predict physical gas saturations. *Geophysical Research Letters*, *44*, 9901–9909. https://doi.org/10.1002/2017GL075123

Hamme, R. C., & Emerson, S. (2004). The solubilities of Ne, Ar and N_2 in freshwater and seawater. *Deep Sea Research Part I: Oceanographic Research Papers*, *51*(11), 1517–1528. https://doi.org/10.1016/j.dsr.2004.06.009

Hamme, R. C., & Emerson, S. R. (2006). Constraining bubble dynamics and mixing with dissolved gases: Implications for productivity measurements and oxygen mass balance. *Journal of Marine Research*, *64*(1), 73–95. https://doi.org/10.1357/002224006776412322

Ho, D. T., Wanninkhof, R., Schlosser, P., Ullman, D. S., Herbert, D., & Sullivan, D. S. (2011). Toward a universal relationship between wind speed and gas exchange: Gas transfer velocities measured with $^3He/SF_6$ during the Southern Ocean Gas Exchange Experiment. *Journal of Geophysical Research*, *116*, C00F04. https://doi.org/10.1029/2010JC006854

Keeling, R. F. (1993). On the role of large bubbles in air-sea gas exchange and supersaturation in the ocean. *Journal of Marine Research*, *51*(2), 237–271. https://doi.org/10.1357/0022240933223800

Liang, J.-H., Deutsch, C., McWilliams, J. C., Baschek, B., Sullivan, P. P., & Chiba, D. (2013). Parameterizing bubble-mediated air-sea gas exchange and its effect on ocean ventilation. *Global Biogoechemical Cycles*, *27*, 1–12. https://doi.org/10.1002/gbc.20080

Liang, J.-H., Emerson, S., D'Asaro, E. A., McNeil, C. A., Harcort, R. R., Sullivan, P. P., et al. (2017). On the role of sea state in determining air-sea gas flux in a winter storm. *Journal of Geophysical Research: Oceans*, *122*, 2671–2685. https://doi.org/10.1002/2016JCO12408

Liss, P. S., & Merlivat, L. (1986). Air-sea gas exchange rates: Introduction and synthesis. In P. Buat-Menard & D. Reidel (Eds.), *The role of air-sea exchange in geochemical cycling* (pp. 113–127). Dordrecht: Springer.

McNeil, C. L., Johnson, B., & Farmer, D. M. (1995). In-situ measurement of dissolved nitrogen and oxygen in the ocean. *Deep Sea Research Part I: Oceanographic Research Papers*, *42*(5), 819–826. https://doi.org/10.1016/0967-0637(95)97829

Merlivat, L., & Memery, L. (1983). Gas exchange across an air-water interface: Experimental results and modeling of bubble contribution to transfer. *Journal of Geophysical Research*, *88*(C1), 707–724. https://doi.org/10.1029/JC088iC01p00707

Nightingale, P. D., Malin, G., Law, C. S., Watson, A. J., Liss, P. S., Liddicoat, M. I., et al. (2000). In situ evaluation of air-sea gas exchange parameterizations using novel conservative and volatile tracers. *Global Biogeochemical Cycles*, *14*(1), 373–387. https://doi.org/10.1029/1999GB900091

Palevsky, H. I., & Quay, P. D. (2017). Influence of biological carbon export on ocean carbon uptake over the annual cycle across the North Pacific Ocean. *Global Biogeochemical Cycles*, *31*, 81–95. https://doi.org/10.1002/2016GB005527

Spitzer, W., & Jenkins, W. (1989). Rates of vertical mixing, gas exchange and new production: Estimates from seasonal gas cycles in the upper ocean near Bermuda. *Journal of Marine Research*, *47*, 69–196.

Stanley, R., Jenkins, W., Lott, D., & Doney, S. (2009). Noble gas constraints on air-sea gas exchange and bubble fluxes. *Journal of Geophysical Research*, *114*, C11020. https://doi.org/10.1029/2009JC005396

Vagle, S., McNeil, C., & Steiner, N. (2010). Upper ocean bubble measurements from the NE Pacific and estimates of their role in air-sea gas transfer of the weakly soluble gases nitrogen and oxygen. *Journal of Geophysical Research*, *115*, C12054. https://doi.org/10.1029/2009JC005990

Wanninkhof, R. (1992). Relationship between wind speed and gas exchange over the ocean. *Journal of Geophysical Research*, *97*(C5), 7373–7382. https://doi.org/10.1029/92JC00188

Wanninkhof, R., Ledwell, J. R., & Broecker, W. S. (1985). Gas exchange-wind speed relation measured with sulfur hexafluoride on a lake. *Science*, *227*(4691), 1224–1226. https://doi.org/10.1126/science.227.4691.1224

Watson, A. J. R., Upstill-Goddard, R. C., & Liss, P. S. (1991). Air-sea exchange in rough and stormy seas measured by a dual tracer technique. *Nature*, *349*(6305), 145–147. https://doi.org/10.1038/349145a0

Woolf, D. K. (1997). Bubbles and their role in gas exchange. In P. S. Liss & R. A. Duce (Eds.), *The sea surface and global change* (pp. 173–206). New York: Cambridge University Press. https://doi.org/10.1017/CBO9780511525025.007

Woolf, D. K., & Thorpe, S. (1991). Bubbles and the air-sea exchange of gases in near saturation conditions. *Journal of Marine Research*, *49*(3), 435–466. https://doi.org/10.1357/002224091784995765

Yang, B., Emerson, S. R., & Pena, A. (2018). The effect of the 2013-2016 high temperature anomaly in the subarctic Pacific (the "Blob") on net community production. *Biogeosciences*, *15*(21), 6747–6759. https://doi.org/10.5194/bg-15-6747-2018

Zhang, X., Lewis, M., Lee, M., Johnson, B., & Korotaev, G. (2002). The volume scattering function of natural bubble populations. *Limnology and Oceanography*, *47*(5), 1273–1282. https://doi.org/10.4319/lo.2002.47.5.1273